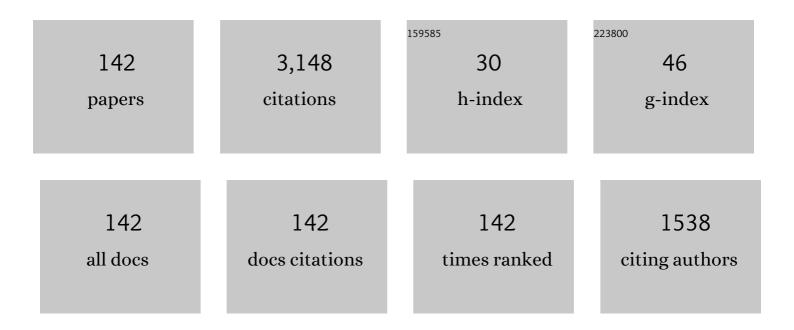
Carlos Paz-Soldan

List of Publications by Year in descending order

Source: https://exaly.com/author-pdf/33259/publications.pdf Version: 2024-02-01



#	Article	IF	CITATIONS
1	DIII-D research advancing the physics basis for optimizing the tokamak approach to fusion energy. Nuclear Fusion, 2022, 62, 042024.	3.5	11
2	Shattered pellet injection experiments at JET in support of the ITER disruption mitigation system design. Nuclear Fusion, 2022, 62, 026012.	3.5	25
3	Controlling the size of non-axisymmetric magnetic footprints using resonant magnetic perturbations. Nuclear Fusion, 2022, 62, 026018.	3.5	4
4	Pellet triggering of edge localized modes in low collisionality pedestals at DIII-D. Nuclear Fusion, 2022, 62, 026017.	3.5	2
5	Physics of runaway electrons with shattered pellet injection at JET. Plasma Physics and Controlled Fusion, 2022, 64, 034002.	2.1	7
6	Dynamic measurement of impurity ion transport in runaway electron plateaus in DIII-D. Physics of Plasmas, 2022, 29, 022503.	1.9	4
7	Influence of triangularity on the plasma response to resonant magnetic perturbations. Nuclear Fusion, 2022, 62, 076031.	3.5	4
8	Toroidal modeling of runaway electron loss due to 3D fields in ITER. Nuclear Fusion, 2022, 62, 066026.	3.5	3
9	Prospects for H-mode inhibition in negative triangularity tokamak reactor plasmas. Nuclear Fusion, 2022, 62, 096020.	3.5	12
10	On the stability and stationarity of the Super H-mode combined with an ion transport barrier in the core. Plasma Physics and Controlled Fusion, 2021, 63, 025017.	2.1	14
11	Impact of shape on pedestal characteristics in the wide pedestal quiescent H-mode in the DIII-D tokamak. Nuclear Fusion, 2021, 61, 036032.	3.5	2
12	Compressional Alfvén eigenmodes excited by runaway electrons. Nuclear Fusion, 2021, 61, 036011.	3.5	10
13	Quasisymmetric Optimization of Nonaxisymmetry in Tokamaks. Physical Review Letters, 2021, 126, 125001.	7.8	8
14	Pedestal collapse by resonant magnetic perturbations. Nuclear Fusion, 2021, 61, 044001.	3.5	7
15	Demonstration of Safe Termination of Megaampere Relativistic Electron Beams in Tokamaks. Physical Review Letters, 2021, 126, 175001.	7.8	41
16	Novel compact hard x-ray spectrometer with MCps counting rate capabilities for runaway electron measurements on DIII-D. Review of Scientific Instruments, 2021, 92, 043517.	1.3	3
17	Influence of up-down asymmetry in plasma shape on RMP response. Plasma Physics and Controlled Fusion, 2021, 63, 065003.	2.1	7
18	Predicting operational windows of ELMs suppression by resonant magnetic perturbations in the DIII-D and KSTAR tokamaks. Physics of Plasmas, 2021, 28, .	1.9	20

#	Article	IF	CITATIONS
19	Toroidal modeling of runaway avalanche in DIII-D discharges. Nuclear Fusion, 2021, 61, 066038.	3.5	2
20	Plasma performance and operational space without ELMs in DIII-D. Plasma Physics and Controlled Fusion, 2021, 63, 083001.	2.1	17
21	Estimate of pre-thermal quench non-thermal electron density profile during Ar pellet shutdowns of low-density target plasmas in DIII-D. Physics of Plasmas, 2021, 28, 072501.	1.9	3
22	First demonstration of full ELM suppression in low input torque plasmas to support ITER research plan using n = 4 RMP in EAST. Nuclear Fusion, 2021, 61, 106037.	3.5	26
23	Impact of negative triangularity plasma shaping on the n = 0 resistive wall mode in a tokamak. Nuclear Fusion, 2021, 61, 096033.	3.5	3
24	Diverted negative triangularity plasmas on DIII-D: the benefit of high confinement without the liability of an edge pedestal. Nuclear Fusion, 2021, 61, 116010.	3.5	20
25	Polarized imaging of visible synchrotron emission from runaway electron plateaus in DIII-D. Physics of Plasmas, 2021, 28, .	1.9	4
26	Results on quiescent and post-disruption runaway electrons studies at Frascati Tokamak Upgrade: RE mitigation via solid deuterium pellets and anomalous Doppler instability. Nuclear Fusion, 2021, 61, 116050.	3.5	4
27	Ballooning instability preventing the H-mode access in plasmas with negative triangularity shape on the DIII–D tokamak. Plasma Physics and Controlled Fusion, 2021, 63, 105006.	2.1	25
28	Passive deconfinement of runaway electrons using an in-vessel helical coil. Nuclear Fusion, 2021, 61, 106033.	3.5	13
29	Self-consistent simulation of resistive kink instabilities with runaway electrons. Plasma Physics and Controlled Fusion, 2021, 63, 125031.	2.1	5
30	Integrated ELM and divertor power flux control using RMPs with low input torque in EAST in support of the ITER research plan. Nuclear Fusion, 2021, 61, 106023.	3.5	16
31	Experimental evidence of runaway electron tail generation via localized helical structure in pellet-triggered tokamak disruptions. Nuclear Fusion, 2021, 61, 104001.	3.5	1
32	A novel path to runaway electron mitigation via deuterium injection and current-driven MHD instability. Nuclear Fusion, 2021, 61, 116058.	3.5	21
33	Development of an integrated core–edge scenario using the super H-mode. Nuclear Fusion, 2021, 61, 126064.	3.5	2
34	MeV range particle physics studies in tokamak plasmas using gamma-ray spectroscopy. Plasma Physics and Controlled Fusion, 2020, 62, 014015.	2.1	27
35	Overview of the SPARC tokamak. Journal of Plasma Physics, 2020, 86, .	2.1	181
36	Optimizing the Super H-mode pedestal to improve performance and facilitate divertor integration. Physics of Plasmas, 2020, 27, 102506.	1.9	13

#	Article	IF	CITATIONS
37	MHD stability and disruptions in the SPARC tokamak. Journal of Plasma Physics, 2020, 86, .	2.1	31
38	Wide Operational Windows of Edge-Localized Mode Suppression by Resonant Magnetic Perturbations in the DIII-D Tokamak. Physical Review Letters, 2020, 125, 045001.	7.8	40
39	Toroidal modeling of runaway electron loss due to 3-D fields in DIII-D and COMPASS. Physics of Plasmas, 2020, 27, 102507.	1.9	15
40	Non-planar coil winding angle optimization for compatibility with non-insulated high-temperature superconducting magnets. Journal of Plasma Physics, 2020, 86, .	2.1	3
41	The role of edge resonant magnetic perturbations in edge-localized-mode suppression and density pump-out in low-collisionality DIII-D plasmas. Nuclear Fusion, 2020, 60, 076001.	3.5	36
42	Empirical scaling of the <i>n</i> = 2 error field penetration threshold in tokamaks. Nuclear Fusion, 2020, 60, 086010.	3.5	19
43	Robustness of the tokamak error field correction tolerance scaling. Plasma Physics and Controlled Fusion, 2020, 62, 084001.	2.1	3
44	Runaway electron seed formation at reactor-relevant temperature. Nuclear Fusion, 2020, 60, 056020.	3.5	23
45	Expanding the parameter space of the wide-pedestal QH-mode towards ITER conditions. Nuclear Fusion, 2020, 60, 092006.	3.5	10
46	Role of 3D neoclassical particle flux in density pump-out during ELM control by RMP in DIII-D. Nuclear Fusion, 2020, 60, 036018.	3.5	23
47	Study of argon expulsion from the post-disruption runaway electron plateau following low-Z massive gas injection in DIII-D. Physics of Plasmas, 2020, 27, .	1.9	20
48	Enhanced helium exhaust during edge-localized mode suppression by resonant magnetic perturbations at DIII-D. Nuclear Fusion, 2020, 60, 054004.	3.5	5
49	Real-time pedestal optimization and ELM control with 3D fields and gas flows on DIII-D. Nuclear Fusion, 2020, 60, 076004.	3.5	12
50	Impurity transport in the pedestal of H-mode plasmas with resonant magnetic perturbations. Plasma Physics and Controlled Fusion, 2020, 62, 095021.	2.1	9
51	Nonlinear modeling of the scaling law for the \$m/n = 3/2\$ error field penetration threshold. Nuclear Fusion, 2020, 60, 076006.	3.5	15
52	Creation and sustainment of wide pedestal quiescent H-mode with zero net neutral beam torque. Nuclear Fusion, 2020, 60, 086005.	3.5	13
53	Modeling plasma toroidal flow profile control via NTV torque with n = 2 3D fields in MAST-U. Nuclear Fusion, 2020, 60, 096026.	3.5	4
54	A new stabilizing regime of tearing mode entrainment in the presence of a static error field. Nuclear Fusion, 2019, 59, 126015.	3.5	4

#	Article	IF	CITATIONS
55	First observation of plasma healing via helical equilibrium in tokamak disruptions. Nuclear Fusion, 2019, 59, 094002.	3.5	3
56	Seeding of neoclassical tearing modes by internal crash events in the ASDEX Upgrade and DIII-D tokamaks. Nuclear Fusion, 2019, 59, 066038.	3.5	6
57	Study of argon assimilation into the post-disruption runaway electron plateau in DIII-D and comparison with a 1D diffusion model. Nuclear Fusion, 2019, 59, 106014.	3.5	14
58	Resistive versus ideal plasma response to RMP fields in DIII-D: roles of <i>q</i> ₉₅ and X-point geometry. Nuclear Fusion, 2019, 59, 086012.	3.5	14
59	Observation of rapid frequency chirping instabilities driven by runaway electrons in a tokamak. Nuclear Fusion, 2019, 59, 124004.	3.5	26
60	MARS-F modeling of post-disruption runaway beam loss by magnetohydrodynamic instabilities in DIII-D. Nuclear Fusion, 2019, 59, 126021.	3.5	26
61	<i>L</i> – <i>H</i> transition trigger physics in ITER-similar plasmas with applied <i>n</i> =  3 perturbations. Nuclear Fusion, 2019, 59, 126010.	magnetic	20
62	Optimizing multi-modal, non-axisymmetric plasma response metrics with additional coil rows on DIII-D. Nuclear Fusion, 2019, 59, 086060.	3.5	8
63	Kink instabilities of the post-disruption runaway electron beam at low safety factor. Plasma Physics and Controlled Fusion, 2019, 61, 054001.	2.1	51
64	The effect of plasma shape and neutral beam mix on the rotation threshold for RMP-ELM suppression. Nuclear Fusion, 2019, 59, 056012.	3.5	35
65	High fusion performance in Super H-mode experiments on Alcator C-Mod and DIII-D. Nuclear Fusion, 2019, 59, 086017.	3.5	48
66	Recent DIII-D advances in runaway electron measurement and model validation. Nuclear Fusion, 2019, 59, 066025.	3.5	13
67	The density dependence of edge-localized-mode suppression and pump-out by resonant magnetic perturbations in the DIII-D tokamak. Physics of Plasmas, 2019, 26, .	1.9	51
68	Edge localized mode suppression and plasma response using mixed toroidal harmonic resonant magnetic perturbations in DIII-D. Nuclear Fusion, 2019, 59, 026012.	3.5	12
69	Low-frequency whistler waves in quiescent runaway electron plasmas. Plasma Physics and Controlled Fusion, 2019, 61, 014007.	2.1	20
70	Dissipation of post-disruption runaway electron plateaus by shattered pellet injection in DIII-D. Nuclear Fusion, 2018, 58, 056006.	3.5	41
71	Stellarator Research Opportunities: A Report of the National Stellarator Coordinating Committee. Journal of Fusion Energy, 2018, 37, 51-94.	1.2	15
72	Helical variation of density profiles and fluctuations in the tokamak pedestal with applied 3D fields and implications for confinement. Physics of Plasmas, 2018, 25, .	1.9	6

#	Article	IF	CITATIONS
73	First Direct Observation of Runaway-Electron-Driven Whistler Waves in Tokamaks. Physical Review Letters, 2018, 120, 155002.	7.8	68
74	Dynamic divertor control using resonant mixed toroidal harmonic magnetic fields during ELM suppression in DIII-D. Physics of Plasmas, 2018, 25, 056102.	1.9	17
75	Resolving runaway electron distributions in space, time, and energy. Physics of Plasmas, 2018, 25, 056105.	1.9	31
76	The role of kinetic instabilities in formation of the runaway electron current after argon injection in DIII-D. Plasma Physics and Controlled Fusion, 2018, 60, 124003.	2.1	34
77	Measurement of toroidal variation in conducted heat loads in locked mode induced disruptions on DIII-D. Physics of Plasmas, 2018, 25, 102502.	1.9	Ο
78	The effects of kinetic instabilities on the electron cyclotron emission from runaway electrons. Nuclear Fusion, 2018, 58, 096030.	3.5	11
79	Role of Kinetic Instability in Runaway-Electron Avalanches and Elevated Critical Electric Fields. Physical Review Letters, 2018, 120, 265001.	7.8	45
80	Interpretation of runaway electron synchrotron and bremsstrahlung images. Nuclear Fusion, 2018, 58, 082001.	3.5	12
81	Magnetic polarization measurements of the multi-modal plasma response to 3D fields in the EAST tokamak. Nuclear Fusion, 2018, 58, 076016.	3.5	10
82	Grassy-ELM regime with edge resonant magnetic perturbations in fully noninductive plasmas in the DIII-D tokamak. Nuclear Fusion, 2018, 58, 106010.	3.5	35
83	Experimental conditions to suppress edge localised modes by magnetic perturbations in the ASDEX Upgrade tokamak. Nuclear Fusion, 2018, 58, 096031.	3.5	73
84	Predict-first experimental analysis using automated and integrated magnetohydrodynamic modeling. Physics of Plasmas, 2018, 25, .	1.9	13
85	Modal analysis of the full poloidal structure of the plasma response to n = 2 magnetic perturbations. Physics of Plasmas, 2018, 25, 072509.	1.9	9
86	Investigation of the role of pedestal pressure and collisionality on type-I ELM divertor heat loads in DIII-D. Nuclear Fusion, 2018, 58, 096023.	3.5	29
87	Use of reconstructed 3D VMEC equilibria to match effects of toroidally rotating discharges in DIII-D. Nuclear Fusion, 2017, 57, 016013.	3.5	11
88	Role of a continuous MHD dynamo in the formation of 3D equilibria in fusion plasmas. Nuclear Fusion, 2017, 57, 076014.	3.5	25
89	Effect of rotation zero-crossing on single-fluid plasma response to three-dimensional magnetic perturbations. Plasma Physics and Controlled Fusion, 2017, 59, 044001.	2.1	16
90	Use of Ar pellet ablation rate to estimate initial runaway electron seed population in DIII-D rapid shutdown experiments. Nuclear Fusion, 2017, 57, 016008.	3.5	12

#	Article	IF	CITATIONS
91	Advances in the steady-state hybrid regime in DIII-D—a fully non-inductive, ELM-suppressed scenario for ITER. Nuclear Fusion, 2017, 57, 116057.	3.5	25
92	Modeling of 3D magnetic equilibrium effects on edge turbulence stability during RMP ELM suppression in tokamaks. Nuclear Fusion, 2017, 57, 116003.	3.5	13
93	Study of Z scaling of runaway electron plateau final loss energy deposition into wall of DIII-D. Physics of Plasmas, 2017, 24, .	1.9	16
94	Avoidance of tearing mode locking with electro-magnetic torque introduced by feedback-based mode rotation control in DIII-D and RFX-mod. Nuclear Fusion, 2017, 57, 016035.	3.5	21
95	Spatiotemporal Evolution of Runaway Electron Momentum Distributions in Tokamaks. Physical Review Letters, 2017, 118, 255002.	7.8	53
96	Impact of ideal MHD stability limits on high-beta hybrid operation. Plasma Physics and Controlled Fusion, 2017, 59, 014027.	2.1	31
97	Impact of toroidal and poloidal mode spectra on the control of non-axisymmetric fields in tokamaks. Physics of Plasmas, 2017, 24, .	1.9	19
98	Validation of the model for ELM suppression with 3D magnetic fields using low torque ITER baseline scenario discharges in DIII-D. Physics of Plasmas, 2017, 24, .	1.9	43
99	A path to stable low-torque plasma operation in ITER with test blanket modules. Nuclear Fusion, 2017, 57, 036004.	3.5	9
100	Effect of thick blanket modules on neoclassical tearing mode locking in ITER. Nuclear Fusion, 2017, 57, 014004.	3.5	7
101	Applying the new gamma ray imager diagnostic to measurements of runaway electron Bremsstrahlung radiation in the DIII-D Tokamak (invited). Review of Scientific Instruments, 2016, 87, 11E602.	1.3	16
102	Interaction of external n  =  1 magnetic fields with the sawtooth instability in low-q RFX-mod ar tokamaks. Nuclear Fusion, 2016, 56, 106012.	nd ₃ .5III-D	13
103	Dependence of neoclassical toroidal viscosity on the poloidal spectrum of applied nonaxisymmetric fields. Nuclear Fusion, 2016, 56, 036008.	3.5	21
104	Equilibrium drives of the low and high field side n  =  2 plasma response and impact on global confinement. Nuclear Fusion, 2016, 56, 056001.	3.5	21
105	The non-thermal origin of the tokamak low-density stability limit. Nuclear Fusion, 2016, 56, 056010.	3.5	5
106	Error field optimization in DIII-D using extremum seeking control. Nuclear Fusion, 2016, 56, 076003.	3.5	11
107	Evidence of Toroidally Localized Turbulence with Applied 3D Fields in the DIII-D Tokamak. Physical Review Letters, 2016, 117, 135001.	7.8	21
108	Identification of multi-modal plasma responses to applied magnetic perturbations using the plasma reluctance. Physics of Plasmas, 2016, 23, .	1.9	19

#	Article	IF	CITATIONS
109	Rotation profile flattening and toroidal flow shear reversal due to the coupling of magnetic islands in tokamaks. Physics of Plasmas, 2016, 23, 056107.	1.9	18
110	Suppression of type-I ELMs with reduced RMP coil set on DIII-D. Nuclear Fusion, 2016, 56, 036020.	3.5	16
111	Landau resonant modification of multiple kink mode contributions to 3D tokamak equilibria. Nuclear Fusion, 2016, 56, 014003.	3.5	4
112	Compatibility of internal transport barrier with steady-state operation in the high bootstrap fraction regime on DIII-D. Nuclear Fusion, 2015, 55, 123025.	3.5	83
113	Three-dimensional equilibria and island energy transport due to resonant magnetic perturbation edge localized mode suppression on DIII-D. Physics of Plasmas, 2015, 22, .	1.9	9
114	Experimental tests of linear and nonlinear three-dimensional equilibrium models in DIII-D. Physics of Plasmas, 2015, 22, .	1.9	40
115	Lack of dependence on resonant error field of locked mode island size in ohmic plasmas in DIII-D. Nuclear Fusion, 2015, 55, 023011.	3.5	4
116	Measurements of the toroidal torque balance of error field penetration locked modes. Plasma Physics and Controlled Fusion, 2015, 57, 025016.	2.1	15
117	Effects of resistivity and rotation on the linear plasma response to non-axisymmetric magnetic perturbations on DIII-D. Plasma Physics and Controlled Fusion, 2015, 57, 025015.	2.1	27
118	Pedestal Bifurcation and Resonant Field Penetration at the Threshold of Edge-Localized Mode Suppression in the DIII-D Tokamak. Physical Review Letters, 2015, 114, 105002.	7.8	141
119	Observation of a Multimode Plasma Response and its Relationship to Density Pumpout and Edge-Localized Mode Suppression. Physical Review Letters, 2015, 114, 105001.	7.8	124
120	The quiescent H-mode regime for high performance edge localized mode-stable operation in future	1.9	45
121	Control of plasma stored energy for burn control using DIII-D in-vessel coils. Nuclear Fusion, 2015, 55, 053001.	3.5	16
122	Measurement of runaway electron energy distribution function during high-Z gas injection into	1.9	50
123	Characterization of MHD activity and its influence on radiation asymmetries during massive gas injection in DIII-D. Nuclear Fusion, 2015, 55, 073029.	3.5	24
124	The role of MHD in 3D aspects of massive gas injection. Nuclear Fusion, 2015, 55, 073032.	3.5	28
125	Decoupled recovery of energy and momentum with correction ofn  =  2 error fields. Nuclear Fus 2015, 55, 083012.	sion. 3.5	22
126	Fast ion transport during applied 3D magnetic perturbations on DIII-D. Nuclear Fusion, 2015, 55, 073028.	3.5	42

#	Article	IF	CITATIONS
127	Feedback-assisted extension of the tokamak operating space to low safety factor. Physics of Plasmas, 2014, 21, .	1.9	14
128	An upgrade of the magnetic diagnostic system of the DIII-D tokamak for non-axisymmetric measurements. Review of Scientific Instruments, 2014, 85, 083503.	1.3	60
129	Tokamak Operation with Safety Factor <mml:math <br="" xmlns:mml="http://www.w3.org/1998/Math/MathML">display="inline"> <mml:mrow> <mml:msub> <mml:mrow> <mml:mi>q </mml:mi> </mml:mrow> <mml via Control of MHD Stability. Physical Review Letters, 2014, 113, 045003.</mml </mml:msub></mml:mrow></mml:math>	:mn7x❸5 <td>mm1l8mn></td>	mm 1l8 mn>
130	The spectral basis of optimal error field correction on DIII-D. Nuclear Fusion, 2014, 54, 073013.	3.5	44
131	The importance of matched poloidal spectra to error field correction in DIII-D. Physics of Plasmas, 2014, 21, .	1.9	39
132	An ITPA joint experiment to study runaway electron generation and suppression. Physics of Plasmas, 2014, 21, .	1.9	71
133	Growth and decay of runaway electrons above the critical electric field under quiescent conditions. Physics of Plasmas, 2014, 21, 022514.	1.9	60
134	Boundary perturbations coupled to core 3/2 tearing modes on the DIII-D tokamak. Plasma Physics and Controlled Fusion, 2013, 55, 095006.	2.1	8
135	Non-axisymmetric magneto- hydrodynamic equilibrium in the presence of internal magnetic islands and external magnetic perturbation coils. Plasma Physics and Controlled Fusion, 2013, 55, 125009.	2.1	2
136	Wall-locking of kink modes in a line-tied screw pinch with a rotating wall. Physics of Plasmas, 2012, 19, 056104.	1.9	4
137	Asymmetric error field interaction with rotating conducting walls. Physics of Plasmas, 2012, 19, 072511.	1.9	3
138	Resistive and ferritic-wall plasma dynamos in a sphere. Physics of Plasmas, 2012, 19, .	1.9	8
139	Two-dimensional axisymmetric and three-dimensional helical equilibrium in the line-tied screw pinch. Physics of Plasmas, 2011, 18, 052114.	1.9	10
140	Stabilization of the Resistive Wall Mode by a Rotating Solid Conductor. Physical Review Letters, 2011, 107, 245001.	7.8	7
141	The rotating wall machine: A device to study ideal and resistive magnetohydrodynamic stability under variable boundary conditions. Review of Scientific Instruments, 2010, 81, 123503.	1.3	7
142	Design and initial operation of multichord soft x-ray detection arrays on the STOR-M tokamak. Review of Scientific Instruments, 2008, 79, 10E926.	1.3	9